Supporting Information for

Atomic insight into Li^+ ion transport in amorphous electrolytes $Li_xAlO_yCl_{3+x-2y}$ ($0.5 \leq x \leq 1.5$, $0.25 \leq y \leq 0.75$)

Qifan Yang[1, 2], Jing Xu[1, 3], Xiao Fu[1, 2], Jingchen Lian[1, 2], Liqi Wang[1, 3], Xuhe Gong[1, 4], Ruijuan Xiao[1, 2, 3, *] and Hong Li[1, 2, 3, *]

[1] Beijing National Laboratory for Condensed Matter Physics, Institute of Physics, Chinese Academy of Sciences, Beijing 100190, China

[2] Center of Materials Science and Optoelectronics Engineering, University of Chinese Academy of Sciences, Beijing 100049, China

[3] School of Physical Sciences, University of Chinese Academy of Sciences, Beijing 100049, China

[4] School of Materials Science and Engineering, Key Laboratory of Aerospace Materials and Performance (Ministry of Education), Beihang University, Beijing 100191, China

E-mail: rjxiao@iphy.ac.cn, hli@iphy.ac.cn

Methods

Structure acquisition: Crystal structure of $LiAlCl_4$ was obtained from Materials Project database. Four different amorphous LAOCs ($Li_{0.5}AlO_{0.75}Cl_2$, $Li_{1.0}AlO_{0.75}Cl_{2.5}$, $Li_{1.5}AlO_{0.75}Cl_3$, $Li_{1.0}AlO_{0.25}Cl_{3.5}$) were obtained by doping with varying concentrations of O in the $LiAlCl_4$ crystal structure as well as removing corresponding amounts of Cl according to charge neutrality, and performing melting and quenching process by AIMD simulations. For comparison, the amorphous structure of $Li_{1.0}AlCl_4$ was also generated using the same method. Figure S3 and S4 prove the successful acquisition of amorphous LAOC structures. The structures were visualized by the VESTA software package[1].

Ab initio molecular dynamics simulation: We performed AIMD simulations and the structural relaxation to construct amorphous structural models and study the structure and ion transport characteristics of LAOCs (Table S1 shows the atom number of each cell) with lattice parameters larger than or near 10 Å, with nonspin-polarized DFT calculations using a Γ-centered k-point. The AIMD calculations was conducted with a Nose thermostat[2] for 30,000 steps at 600K (melting); 3,000 steps from 600K to 300K (quenching), and 50,000 steps at 300K (equilibrium) using a time step of 1 fs. The last configuration of the quenching process is adopted to perform the structural relaxation by density functional theory (DFT) computation to obtain the cell parameters through Vienna Ab initio Simulation Package (VASP)[3] and Perdew–Burke–Ernzerhof (PBE)[4], gradient approximation (GGA) by the projector-augmented-wave (PAW) approach. The cutoffs of the wavefunction and the density are 520 eV and 780 eV, respectively. Both cells and ions were relaxed to reach the energy and force convergence criterion of 10^{-5} eV and 0.01 eV/Å. For equilibrium process, the first 10 ps is used for equilibrating the structure, and the subsequent 40 ps is used for statistically obtaining the ion migration properties. We carried out all analysis by pymatgen and the pymatgen-diffusion Python packages.[5], [6]

MLIP-based molecular dynamics simulation: The MLIP model was trained by DeepMD[7] with the training set of AIMD simulation data of the original crystal structure of $Li_{1.0}AlO_{0.75}Cl_{2.5}$ each 30ps at 300K, 400K, 500K and 600K, using the descriptor "se_e2_a" and parameters derived from the examples provided by the DeePMD framework. The MD simulations of $Li_{1.0}AlO_{0.75}Cl_{2.5}$ by LAMMPS[8] (Large-scale Atomic/Molecular Massively Parallel Simulator) in original cell, 2×2×2 cell and 3×3×3 cell (Table S2 shows the atom number of each cell) were conducted at constant volume and temperature (NVT) ensemble. The MD simulation was carried out for 500,000 steps at 300K for original cell and 2×2×2 cell, with a time step of 0.1 fs. For 3×3×3 cell, Model 1 refers to the MD run for 3,000,000 steps (300 ps) at 600K (melting); 30,000 steps (3 ps) from 600K to 300K (quenching) and 5,000,000 steps (500 ps) at 300K (equilibrium), with a time step of 0.1 fs; Model 2 refers to the MD run for 5,000,000 steps (500 ps) at 300K, with a time step of 0.1 fs. For MD of Model 1 and 2 at 300K, the 0 ps to 500 ps is used for further analysis. The results of them were used to verify the accuracy of the model, study size effects and investigate structural and ion conducting characteristics in large boxes. We carried out all analysis by pymatgen and the pymatgen-diffusion Python packages. The open visualization tool (OVITO)[9] was used for the visualizing and analyzing of LAMMPS results.

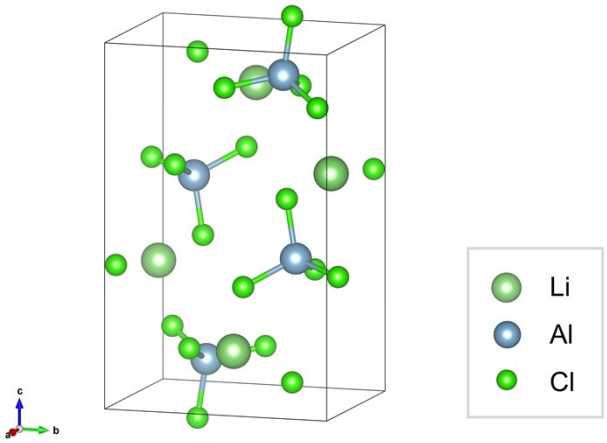

Figure S1. The structure of crystalline $LiAlCl_4$.

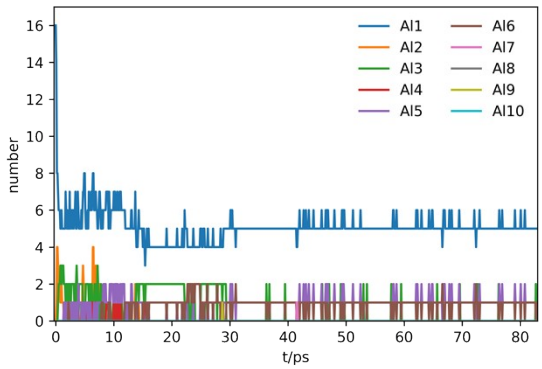

Figure S2. The variation of the number of Al-chains with different lengths over the whole AIMD simulation for $Li_{1.0}AlO_{0.75}Cl_{2.5}$ (30 ps at 600K (melting); 3 ps from 600K to 300K (quenching) and 50 ps at 300K (equilibrium).

It is found that the distribution of chain length changed basically only in the melting process.

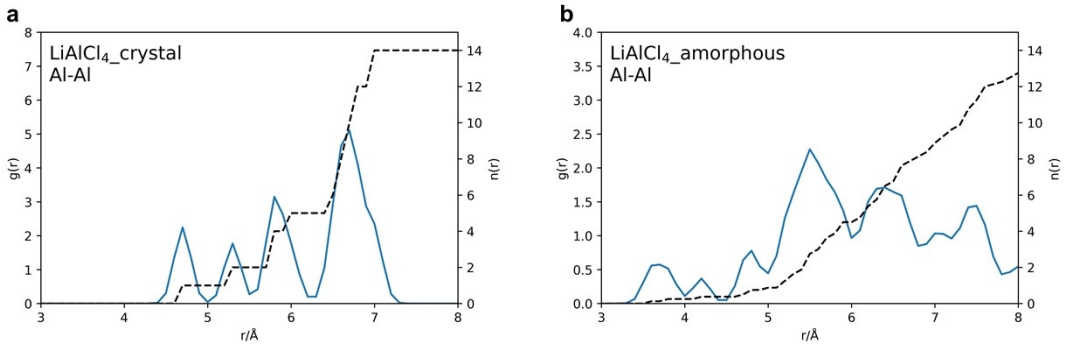

Figure S3. The RDF curves for Al-Al pairs of crystal and amorphous $LiAlCl_4$ at 300K.

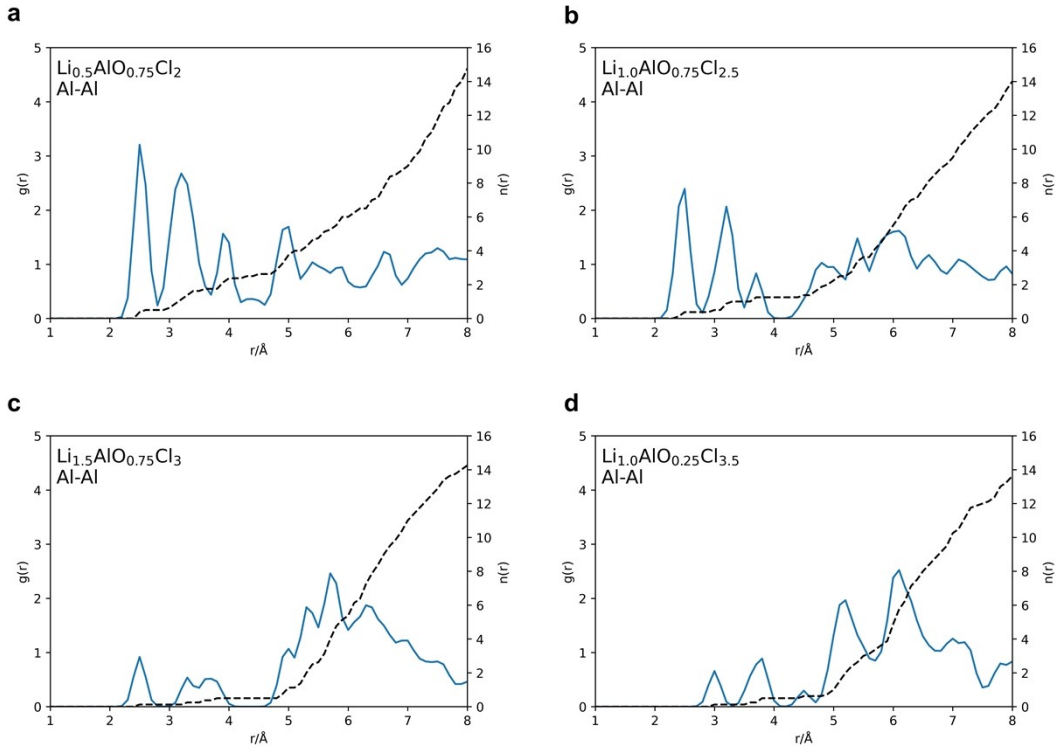

Figure S4. The RDF curves for Al-Al pairs of amorphous LAOCs at 300K.

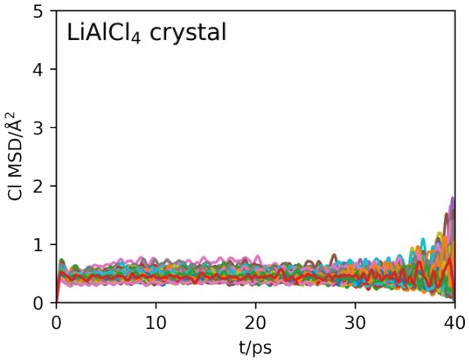

Figure S5. MSD of each Cl atom for crystal $LiAlCl_4$ calculated by AIMD at 300K.

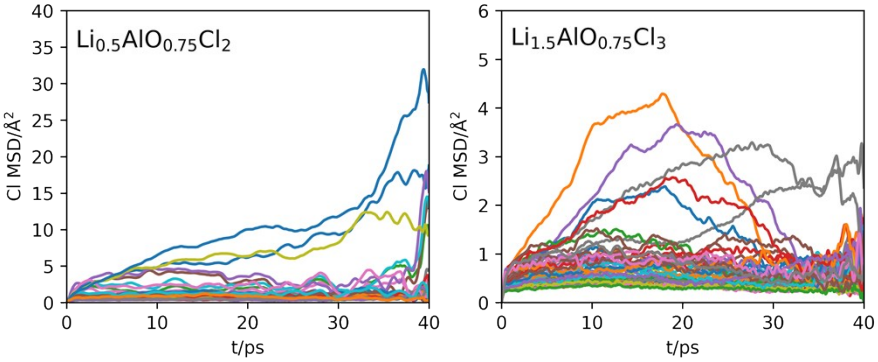

Figure S6. MSD of each Cl atom for $Li_{0.5}AlO_{0.75}Cl_2$ and $Li_{1.5}AlO_{0.75}Cl_3$ calculated by AIMD at 300K.

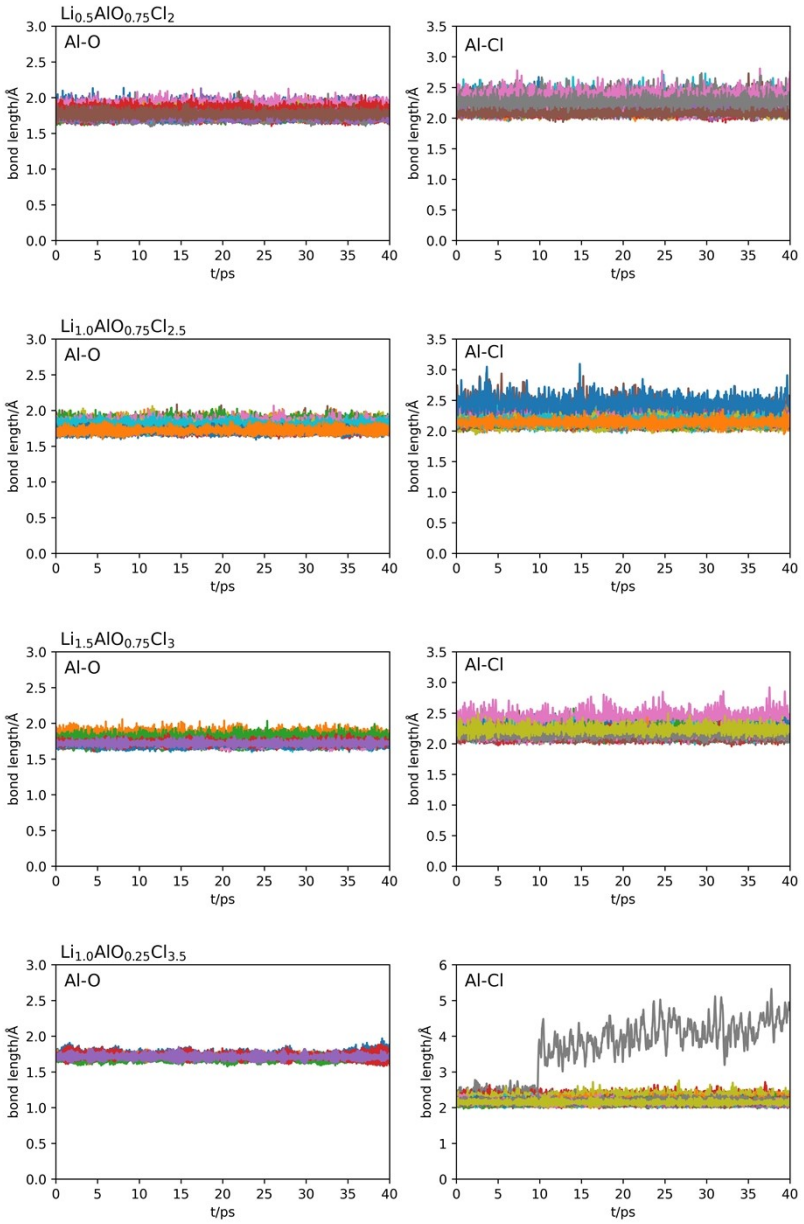

Figure S7. The Al-O and Al-Cl bond length over AIMD simulation at 300K of LAOCs.

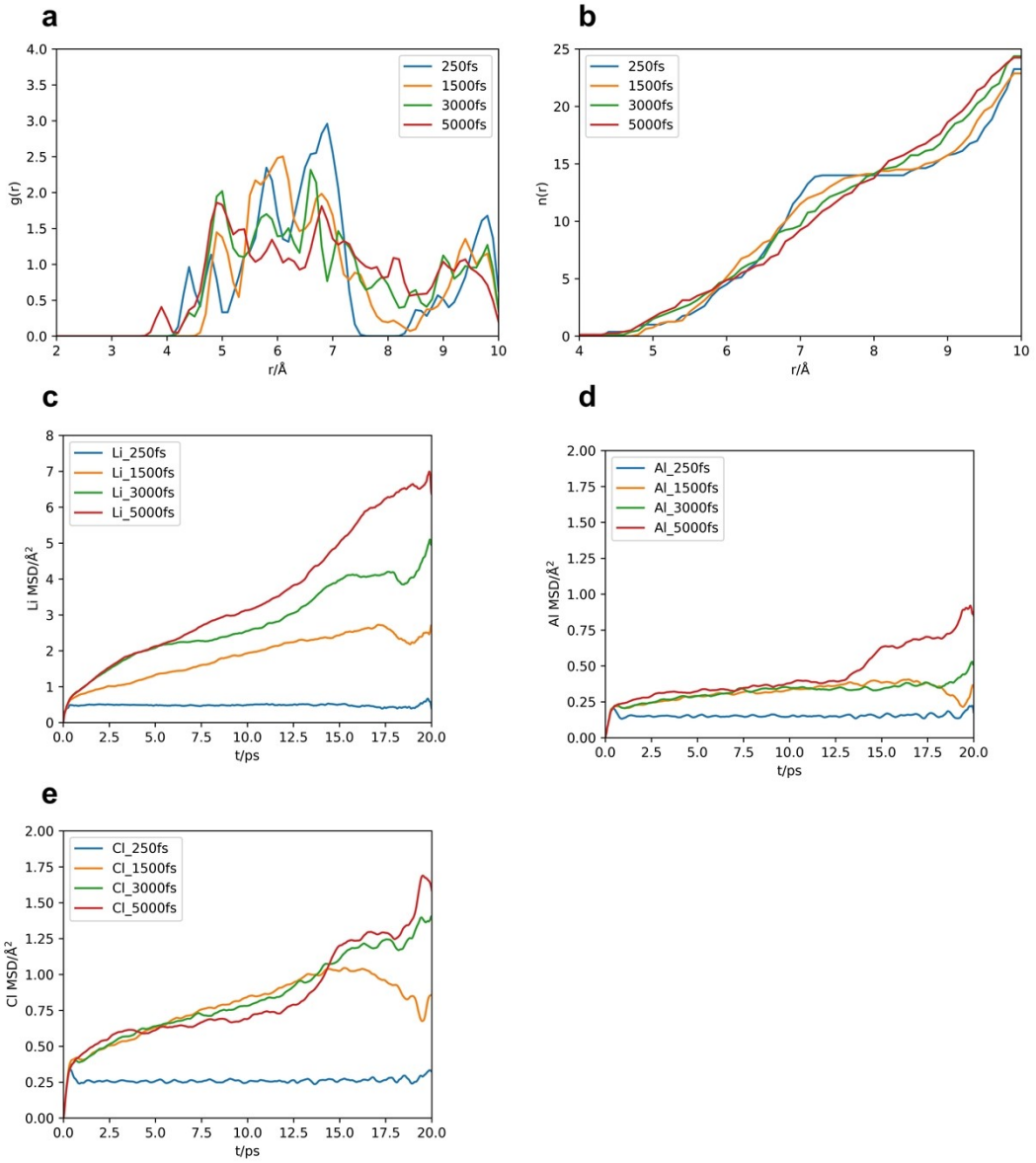

Figure S8. (a) The RDFs and (b) The coordination numbers integrated from RDFs for Al-Al pairs of the $LiAlCl_4$ structures with different melting times. (c) The Li MSDs of the $LiAlCl_4$ structures with different melting times at 300K within the range of 11-50ps. (d). The Al MSDs of the $LiAlCl_4$ structures with different melting times at 300K within the range of 11-50ps. (e). The Cl MSDs of the $LiAlCl_4$ structures with different melting times at 300K within the range of 11-50ps.

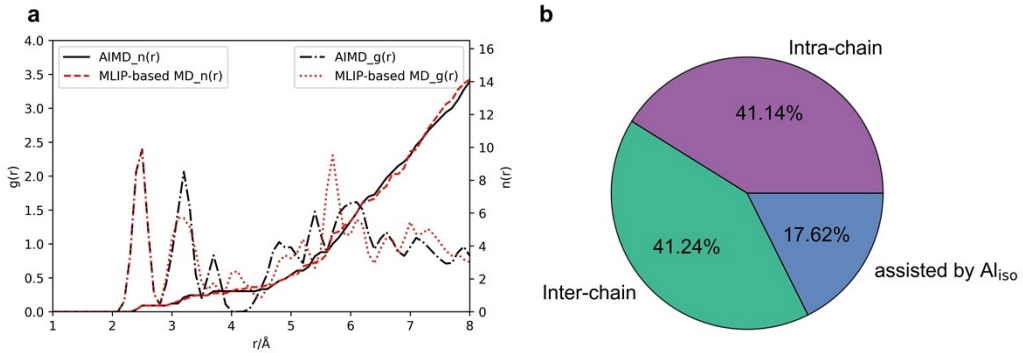

Figure S9. (a). The Al-Al RDF and coordination number curves of the $Li_{1.0}AlO_{0.75}Cl_{2.5}$ original cell by AIMD and MLIP-based MD. (b). The percentage of three different transport events in $Li_{1.0}AlO_{0.75}Cl_{2.5}$ with MLIP-based MD simulation at 300K within the range of 11-50ps.

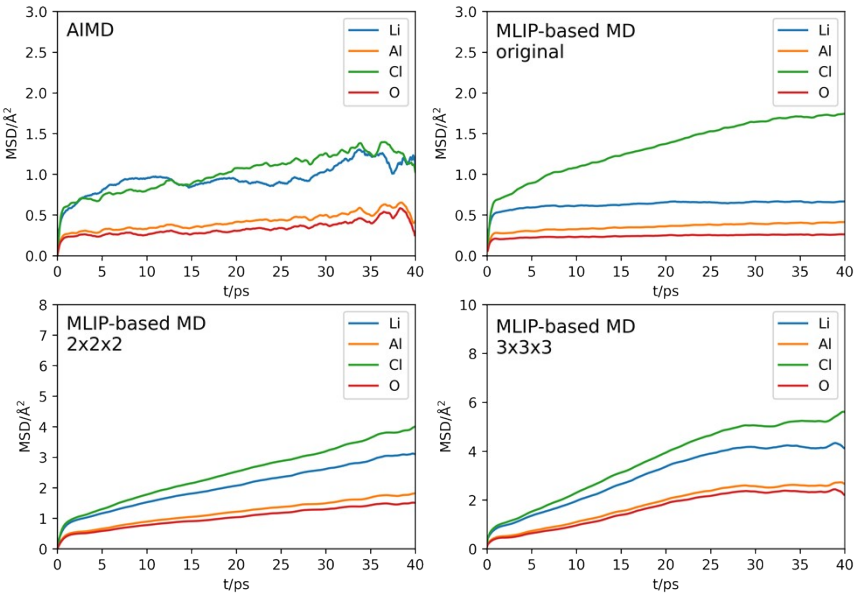

Figure S10. The MSDs at 300K of $Li_{1.0}AlO_{0.75}Cl_{2.5}$ by AIMD and different cell sizes by MLIP - based MD.

Table S1. Total number of atoms in cells for AIMD simulations.

Structure	Total Number of Atoms in Cell
crystal $LiAlCl_4$	96
$Li_{1.0}AlCl_4$	96
$Li_{0.5}AlO_{0.75}Cl_2$	68
$Li_{1.0}AlO_{0.75}Cl_{2.5}$	84
$Li_{1.5}AlO_{0.75}Cl_3$	100
$Li_{1.0}AlO_{0.25}Cl_{3.5}$	92

Table S2. Total number of atoms in cells of $Li_{1.0}AlO_{0.75}Cl_{2.5}$ for MLIP-based MD simulation.

Structure	Total Number of Atoms in Cell
original cell	84
2×2×2 cell	672
3×3×3 cell	2268

Note S1. The specific statistical methods and processes of the migration of Li^+ ions in LAOC structures.

The data statistics are conducted by writing Python codes to read and analyze the atomic structures at each moment during AIMD simulations. The detailed processes used for the statistics for each Figure are as follows:

(1) For Figure 2b: To determine whether Li has migrated and what type of migration has occurred by counting the type of the nearest Al atom to each Li at each moment during the AIMD simulations. When the Al atom closest to Li changes, a Li migration event occurs, and the type of Al atom before and after migration is used to determine what kind of migration event has occurred.

(2) For Figure 2c: We obtained the results of the right column by statistically analyzing the AOC tetrahedra where the Li ion's nearest Al atom is located during all Li migration events in the AIMD simulations.

(3) For Figure 2d: We have counted the types of AOC on which Cl atoms with MSD>5 $Å^2$ (in $Li_{0.5}AlO_{0.75}Cl_2$, $Li_{1.0}AlO_{0.75}Cl_{2.5}$ and $Li_{1.0}AlO_{0.25}Cl_{3.5}$) or >1 $Å^2$ (due to the poorer rotation of Cl atoms in $Li_{1.5}AlO_{0.75}Cl_3$) are located during the AIMD simulations.

Note S2. Verification of the accuracy of MLIP model and the study on the size effect.

Firstly, the accuracy of this model was evaluated. AIMD simulations and MLIP-based MD simulations of the $Li_{1.0}AlO_{0.75}Cl_{2.5}$ original cell at 300K were conducted respectively for evaluating the rationality of the model. The Al-Al RDF of each structure is adopted to analyze the similarity among structures. As we can see in Figure S9a, the Al-Al RDF and coordination number curves of the two structures, especially the first nearest neighbor coordination, are very similar, so it can be considered that their structures are basically homologous. In addition, the accuracy of the model can be verified by comparing the statistical results of ion transport events between two different structures. Statistical results in Figure S9b is very similar to that of $Li_{1.0}AlO_{0.75}Cl_{2.5}$ in Figure 2b, indicating the two simulation processes reveal the same migration characteristics. Additionally, the MSDs in AIMD simulation and MLIP-based MD are similar in original cell, which further proves the reliability of the model. Therefore, the effectiveness of the MLIP model as well as the consistency of AIMD and MLIP-based MD for structures are demonstrated from three aspects: structure, migration events, and MSD. Secondly, the size effect of the MLIP model was explored by conducting MLIP-based MD simulation of the $Li_{1.0}AlO_{0.75}Cl_{2.5}$ original cell, the expanded 2×2×2 and 3×3×3 cell at 300K. By Figure S10, it can be deduced that the MSDs of 2×2×2 and 3×3×3 cell already formed a good convergence, so we chose 3×3×3 cell to conduct more MLIP-based MD simulations for the following analysis.

Note S3. Simulation Process of Model 1 and Model 2.

There are two different model building methods: Model 1 refers to MLIP-based MD calculations of a process of re-melting for 300ps at 600K, quenching for 3ps from 600K to 300K, and equilibrating for 500 ps at 300K; Model 2 refers to the direct conduction of MLIP-based MD simulations on the expanded structure for 500 ps at 300K.

---

[1] K. Momma and F. Izumi, *J Appl Crystallogr*, 2011, **44**, 1272-1276.

[2] S. Nose, *Theor. Phys. Suppl.*, 1991, 1-46.

[3] G. Kresse and J. Furthmuller, *Comput. Mater. Sci.*, 1996, **6**, 15-50.

[4] J.P. Perdew, K. Burke and M. Ernzerhof, *Phys Rev Lett.*, 1996, **77**, 3865-3868.

[5] S.P. Ong, W.D. Richards, A. Jain, G. Hautier, M. Kocher, S. Cholia, D. Gunter, V.L. Chevrier, K.A. Persson and G. Ceder, *Comput. Mater. Sci.*, 2013, **68**, 314-319.

[6] Z. Deng, Z.Y. Zhu, I.H. Chu and S.P. Ong, *Chem. Mater.*, 2017, **29**, 281-288.

[7] H. Wang, L.F. Zhang, J.Q. Han and W.N. E, *Comput Phys Commun*, 2018, **228**, 178-184.

[8] S. Plimpton, *J. Comput. Phys.*, 1995, **117**, 1-19.

[9] A. Stukowski, *Model Simul Mat Sci Eng*, 2010, **18**, 015012.